PERGAMON

International Journal of Heat and Mass Transfer 45 (2002) 3413–3427

International Journal of HEAT and MASS TRANSFER

www.elsevier.com/locate/ijhmt

Experimental estimation of the transient free convection heat transfer coefficient on a vertical flat plate in air

Gaël Maranzana, Sophie Didierjean, Benjamin Rémy, Denis Maillet *

Laboratoire d'Energétique et de Mécanique Théorique et Appliquée, Institut National Polytechnique de Lorraine, Université Henri Poincaré, U.M.R. 7563 CNRS, 2 Avenue de la Forêt de Haye, 54 504 Vandoeuvre-Les-Nancy, France

Received 23 May 2001; received in revised form 15 December 2001

Abstract

Transient heat convection on a vertical plate has been interpreted both theoretically and experimentally, in terms of a variable heat transfer coefficient, by several authors. Few results concern the case were air is the fluid. Joule heating of a very thin vertical graphite foil has been tested experimentally here. Two different methods of inversion have been studied for estimating the local or global transfer coefficient, starting from infrared camera measurements. The second method has been able to provide the convective contribution to the measured global transfer coefficient. Experimental results with different levels of heating show that the early transfer coefficient decrease proportionally (in time t) to t^{-1}, and not to $t^{-1/2}$ as the early times conduction theory would anticipate. Other effects than those already presented in the literature remain to be investigated, in order to explain the discrepancy of this theory for air.

Relaxation experiments show that enhancement of the wall/air exchange by a mastering of the transient heating of the whole wall seems to be quite difficult to obtain

1. Introduction

The definition of the natural or forced convection heat transfer coefficient is strongly linked to the notion of steady state regime where heat transfer correlations based on a dimensional analysis can be defined. In many practical situations, such as electronic circuits cooling or heat exchangers, the characterization of the transient behaviour of the wall/fluid heat exchange is of prime importance, either to model the thermal system or to improve (or to reduce) the heat fluxes. The use of steady state heat transfer coefficients is generally extended to conditions where both the wall temperature and the temperature outside the boundary layer vary slowly with time. In these 'quasi steady' situations the heat capacity of the boundary layer is low enough to justify this kind of assumption. If however fast regimes are considered, such as natural convection caused by a step heating of a semi infinite vertical wall, this notion of proportionality between the instantaneous wall heat flux density and the temperature difference between wall and outside fluid *at the same time* loses its intrinsic character: in this type of thermal regime, the wall heat flux does not depend on this instantaneous temperature difference, but also on the history of this difference since the time an initial temperature disequilibrium has been set.

Such situations have been studied first by Siegel [1]: he investigated analytically the boundary layer growth when a semi-infinite vertical plate was subjected to a step heating (uniform imposed temperature or heat flux density). Three types of regimes were described: for short times t or points far from the leading edge (large x), the local heat transfer coefficient h is produced by purely one-directional heat condition in the direction perpendicular to the plate (no height dependance of $h : h = h(t)$). For long times, a steady state regime appears: $h = h(x)$. For intermediate times or heights, this coefficient depends both on time and space: $h = h(t, x)$. Goldstein and Eckert [2] validated experimentally this analysis for uniform imposed flux conditions in water using a

* Corresponding author. Tel.: +33-03-83-59-56-06; fax: +33-03-83-59-55-31.

E-mail address: dmaillet@ensem.inpl-nancy.fr (D. Maillet).

0017-9310/02/$ - see front matter
PII: S0017-9310(02)00049-2

Nomenclature

$\boldsymbol{A}$	matrix
Bi	Biot number of the foil ($= he/\lambda$)
D	copper bar thickness
E	copper bar width
E_{sw}	incident radiation in the short wave band
H	foil height
K_1	temperature derivative of the calibration law of the camera
K_{sw}	calibration constant
K	constant of the coupled conductive model ($= b_{air}/\rho ce$)
L	foil half width
L'	half width of the measured area of the foil
$\boldsymbol{M}$	convolution matrix
N	number of harmonics at truncation
Ra	Rayleigh number ($= (g\mathrm{L}^4\, q_\infty)/(T_m\lambda_{air} \times a_{air}\nu_{air})$)
R_0	electrical resistance of the shunt
$\boldsymbol{S}$	matrix
T	local temperature
T_y	average foil temperature in the thickness (y) direction
T_{yz}	average foil temperature in the thickness (y) and width (z) directions
T_{xyz}	average temperature of the foil ($= \bar{T}$)
$\bar{T}$	same definition as T_{xyz}
$\bar{\boldsymbol{T}}^*$	column vector of the normalized temperatures $\bar{T}^*(t_i)$
T_0	constant temperature
T_m	film temperature (°C)
V	electrical tension
V_p	potential difference of the foil
V_s	potential difference of the shunt
V^o	response of the camera to a blackbody emitting surface
ΔV	variation of the camera's signal
$\boldsymbol{V}$	column vector of the signal V_i at different times t_i
$\mathbf{X}_0$	sensitivity matrix for the net average flux density entering the foil
$\mathbf{X}_n$	sensitivity matrix for the nth harmonic of the flux density at different times
a	thermal diffusivity of the foil
a_{air}	thermal diffusivity of air
b_{air}	thermal effusivity of air
c	specific heat of the foil
e	thickness of the foil
g	gravity
h	heat transfer coefficient
h_t	time part of $h(t,x)$ – see Eq. (17a)
h_x	space part of $h(t,x)$ – see Eq. (17a)
h_n	harmonic of rank n of $h_y(y)$
$\bar{h}$	global heat transfer coefficient
p	Laplace parameter
q	heating power surface density
t	time
Δt	acquisition time step of the camera
u	integration (dumb) variable in time
w	heating power volume density
x, y, z	coordinates in the three directions of the foil
Δy	vertical space step of the thermographic frame

Greek symbols

Θ	absolute temperature (in Kelvin)
Θ_0	initial absolute temperature
Θ_m	absolute film temperature ($= (\Theta + \Theta_0)/2$)
α_n	nth eigenvalue ($= n\pi/H$)
β_i	net power surface density entering the foil at time t_i
$\boldsymbol{\beta}$	column vector of the β_is
δ	thickness of the air thermal boundary layer
δ_{0n}	Kronecker Symbol
ε	emissivity
ϕ_n	nth harmonic of the cosine transform of the wall heat flux density at time t
ϕ_n	column vector of the $\phi_n(t_i)$s (for a fixed n)
ϕ	column vector of the ϕ_ns at a given time
φ	wall heat flux density
φ_z	average wall heat flux density in the width (z) direction
φ_{xz}	average wall heat flux density in the height (x) and width (z) directions ($= \bar{\varphi}$)
$\bar{\varphi}$	same definition as φ_{xz}
φ_0	constant flux density
λ	conductivity in the foil's plane
$\lambda_x, \lambda_y, \lambda_z$	conductivities in the three directions of the foil
λ_{air}	conductivity of air
ν_{air}	kinematic viscosity of air
ρ	mass density of the foil
ρ_e	electric resistivity of the foil
τ_c	characteristic conduction time of the foil ($= e^2/a$)
τ_∞	characteristic convection time of the foil ($= \rho ce/\bar{h}_\infty$)
θ_n	nth harmonic of the cosine transform of the wall temperature T_{xz} at time t
θ_n	column vector of the $\theta_n(t_i)$s (for a fixed n)
σ	standard deviation of the temperature noise
$\bar{\sigma}$	Stefan Boltzmann' s constant

Subscripts

conv	convective
exp	experimental
i	relative to time t_i

lw	long wave	*Superscripts*	
max	maximum value	$*$	normalized value
min	minimum value	o	relative to a blackbody surface
n	relative to harmonic number n	$-$	average value over the foil's surface
sw	short wave	$\tilde{C}$	Laplace transform of C, for $C = T, q, \varphi$
∞	steady state value (long times)	$\hat{C}$	estimated value of C, for $C = \tau_\infty, \bar{\varphi}, \bar{h}, \ldots$

Zender-Mach interferometer. In these experiments the first regime (pure conduction in water) lasted about 30 s. The asymptotic analytic solutions for more general types of thermal excitations (conduction regime) were derived later on by Menold and Kwan-Tzu [3] and Schetz and Eichhorn [4]. Goldstein and Briggs [5] studied the transient regime for both vertical plates and cylinders (step temperature change).

Gebhart [6–8] investigated the same kind of situations but paid a particular attention to the thermal capacity effect of the wall. He extended the classical assumption of self similar temperature and velocity distributions of the steady state boundary layer to the transient regime [6,7]. He published experimental results for transient heating of a vertical metal foil in air – Gebhart and Adams [8] – and for corresponding heating and cooling (relaxation regime) of a composite vertical plate in water – Gebhart [9] and Sammakia et al. [10]. Joshi and Gebhart [11] presented later on a theoretical and experimental analysis where the transient regime was caused by a sudden change of thermal dissipation level in the wall, that is the passing from one steady natural convection regime to a new one (vertical plate in water). A detailed study of the flow and temperature field was presented.

According to our knowledge, all the reported experiments for the measurements of the transfer coefficient in transient natural convection over a vertical flat plate [2] are related to water. The corresponding Gebhart's experiments for air [8] are not analysed in terms of flux dissipation or in terms of a transient h coefficient.

We have decided here to measure the time variation of this coefficient in air by infrared thermography, associated with an inverse analysis, to take into account the thermal presence of the foil where heat is dissipated by Joule effect. This kind of inversion will be implemented without any particular assumption on the type of flow induced by this heating. Another aspect that will be investigated is the possibility to increase the rate of flow by different kinds of uniform transient heating of the wall.

Section 2 will present the experimental setup. The direct model will be derived in Section 3 and two types of inversion procedures will be considered in Section 4. The three classical coupling models between wall and fluid (first 'conduction' phase) will be recalled in Section 5, while simulated data will be used to assess our inversion procedure in Section 6. The experimental results will be presented and analysed in Section 7.

2. Experimental setup

A sketch that gives the main characteristics of the setup is shown in Fig. 1. A graphite foil of thickness $2e = 0.1$ mm, height $H = 100$ mm and width $2L =$

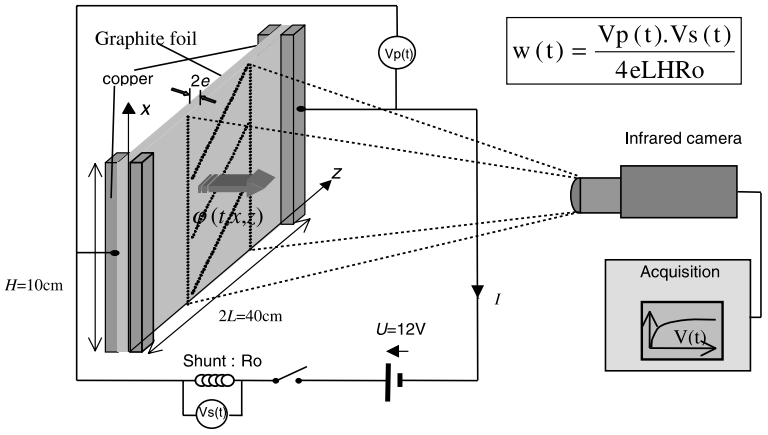

Fig. 1. Experimental setup.

400 mm, is held tight vertically thanks to four copper bars of rectangular cross sections $E \times D = 1$ mm $\times$ 10 mm. The horizontal plane solid surface of the bench is located about 25 cm below the lower edge of the foil.

This foil can be electrically heated, by Joule effect in its volume (electric resistivity $\rho_e = 1300$ μΩ cm). Once the switch closed, the copper bars are connected to a 12 V electric battery. They allow a uniform distribution of the electric potential in the vertical direction in the foil. The electrical power dissipated in the foil is monitored by a numerical oscilloscope. An infrared camera is set in front of one face of the foil. It allows to record the thermal field and, under some assumptions, the surface temperature of one of its faces.

3. Direct model and simulation

3.1. Direct model

One assumes that, once the heating starts, the two faces of the foil behave the same way, which means that no flux flows through the vertical plane of symmetry $y = 0$ (see Fig. 2). One also assumes a similar thermal boundary condition for the other vertical plane of symmetry ($z = 0$) normal to the foil's plane. Because of these assumptions, only a quarter of the foil needs to be considered. The heat diffusion problem in this coordinate system can by written:

$$\lambda_x \frac{\partial^2 T}{\partial x^2} + \lambda_y \frac{\partial^2 T}{\partial y^2} + \lambda_z \frac{\partial^2 T}{\partial z^2} + w(t) = \rho c \frac{\partial T}{\partial t}, \tag{1a}$$

$$-\lambda_y \frac{\partial T}{\partial y} = 0 \quad \text{at } y = 0, \tag{1b}$$

$$-\lambda_y \frac{\partial T}{\partial y} = \varphi(x,z,t) \quad \text{at } y = e, \tag{1c}$$

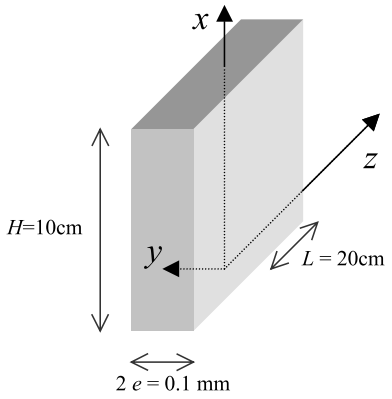

Fig. 2. System of coordinates.

$$-\lambda_x \frac{\partial T}{\partial x} = 0 \quad \text{at } x = 0 \text{ and } x = H, \tag{1d}$$

$$-\lambda_z \frac{\partial T}{\partial z} = 0 \quad \text{at } z = 0 \text{ and } z = L, \tag{1e}$$

$$T = 0 \quad \text{for } t = 0, \tag{1f}$$

where $w(t)$ designates the heating power density (W m^{-3}), λ_x, λ_y, and λ_z the graphite conductivities in the three directions, ρc its volumetric heat, and $\varphi(x,z,t)$ the total local heat flux density of the heat losses (natural convection and radiation) on the front face. We have assumed here that the system is at thermal equilibrium before heating starts at $t = 0$ (this is taken as the reference temperature). Problem (1a)–(1h) can be integrated in the thickness (y) direction, as well as in the horizontal (z) direction:

$$T_y(x,z,t) = \frac{1}{e}\int_0^e T(x,y,z,t)\,\mathrm{d}y, \tag{1g}$$

$$T_{yz}(x,t) = \frac{1}{L}\int_0^L T_y(x,z,t)\,\mathrm{d}z, \qquad \varphi_z(x,t) = \frac{1}{L}\int_0^L \varphi(x,z,t)\,\mathrm{d}z, \tag{1h}$$

which gives

$$\frac{\partial^2 T_{yz}}{\partial x^2} + \frac{q(t) - \varphi_z(x,t)}{\lambda e} = \frac{1}{a}\frac{\partial T_{yz}}{\partial t} \tag{2a}$$

with

$$\frac{\partial T_{yz}}{\partial x} = 0 \quad \text{at } x = 0 \text{ and } x = H, \tag{2b}$$

$$T_{yz} = 0 \quad \text{for } t = 0, \tag{2c}$$

where $\lambda = \lambda_x = \lambda_z$ is the conductivity of graphite in the foil's plane (it is assumed to be isotropic in this plane because of the manufacturing process). $a = \lambda/\rho c$ is its in-plane diffusivity and $q(t) = e\ w\ (t)$ is the heating power density on a unit surface basis.

In practice, in order to take into account the possible z component flux at the foil/copper bar interface, integration (1f) can be implemented on a width L' smaller than the L width – see Fig. 2.

Problem (2a)–(2c) can be finally integrated in the vertical (x) direction, where we get a lumped-body model

$$\frac{\mathrm{d}T_{xyz}}{\mathrm{d}t} = \frac{\rho c}{e}[q(t) - \varphi_{xz}(t)] \tag{3a}$$

with

$$T_{xyz} = 0 \quad \text{for } t = 0 \tag{3b}$$

and

$$T_{xyz}(t) = \int_0^H T_{yz}(x,t)\,\mathrm{d}x \quad \text{and}$$
$$\varphi_{xz}(t) = \frac{1}{H}\int_0^H \varphi_z(x,t)\,\mathrm{d}x. \tag{3c}$$

Under steady state conditions, near ambient temperature, the global exchange coefficient h, associated with the heat loss flux φ_{xz}, has a value of the order of 10 W m^{-2} K^{-1} for air. If we take into account the high conductivity ($\lambda_y = 120$ W m^{-1} K^{-1}) of graphite and its volumetric heat capacity ($\rho c = 7.12 \times 10^5$ J m^{-3} K^{-1}), one finds:

- a Biot number

$$Bi = \frac{he}{\lambda} \approx 4.2 \times 10^{-6} \ll 1,$$

- a characteristic conduction time in the thickness direction

$$\tau_c = \frac{e^2}{a} \approx 15\ \mu\text{s}.$$

This shows that, at any location (x,z) the graphite foil can be considered as having a uniform temperature in its thickness, for both steady state and transient regimes (for $t > \tau_c$). This means that the T_y average temperature – see Eq. (1g) – is the same as the surface temperature T (at $y = e$). This temperature can be measured by the infrared camera in a non-intrusive way. Both systems (2a)–(2c) and (3a)–(3c) can be solved analytically.

Solution of system (2a)–(2c): An integral transformation of Eq. (2a), using the x-direction eigenfunctions $\cos(\alpha_n x)$ yields

$$\frac{\mathrm{d}\theta_n}{\mathrm{d}t} + a\,\alpha_n^2\,\theta_n = \frac{1}{\rho c e}\left(\delta_{0n} H\,q(t) - \phi_n(t)\right), \tag{4a}$$

where θ_n and ϕ_n are the transforms of the surface temperature and of the heat loss flux density, respectively:

$$\theta_n(t) = \int_0^H T_{yz}(x,t)\cos(\alpha_n x)\,\mathrm{d}x,$$
$$\phi_n(t) = \int_0^H \varphi_z(x,t)\cos(\alpha_n x)\,\mathrm{d}x \tag{4b}$$

with

$$\alpha_n = \frac{n\pi}{H} \quad \text{for } n = 0, 1, 2\ldots$$

and δ_{0n} the Kronecker symbol.

Integration of Eq. (4a) for each harmonic provides the surface temperature T variation with x and t (this temperature will be expressed without its subscripts y and z now on):

$$T(x,t) = T_{yz}(x,t) = \frac{1}{H}\left(\theta_0(t) + 2\sum_{n=1}^{\infty}\theta_n(t)\cos(\alpha_n x)\right) \tag{4c}$$

with

$$\theta_0(t) = \frac{1}{\rho c e}\int_0^t \left(H\,q(u) - \phi_0(u)\right)\mathrm{d}u, \tag{4d}$$

$$\theta_n(t) = -\frac{1}{\rho c e}\int_0^t \phi_n(u)\exp(-a\alpha_n(t-u))\,\mathrm{d}u \quad \text{for } n \geq 1. \tag{4e}$$

Solution of system (3a)–(3c): If one notices that the fundamental term $\theta_0(t)$ is equal, by definition, to $HT_{xyz}(t)$ – see Eq. (4b) – the solution of system (3a)–(3c) is

$$\bar{T}(t) = T_{xyz}(t) = \frac{1}{\rho c e}\int_0^t \left(q(u) - \bar{\varphi}(u)\right)\mathrm{d}u, \tag{5}$$

where $\bar{\varphi}(t)$ and $\bar{T}(t)$ stand for the average values of the heat loss flux density and of the temperature over the vertical [0 H] interval.

4. Inversion procedure

4.1. Thermographic signal and temperature variation

When aiming at a (x,z) spot of a radiatively black surface the infrared camera we use (AGEMA 782 short wave) delivers a tension signal of the form

$$V^{\circ}(\Theta) = \frac{A}{e^{B/\Theta} - 1}, \tag{6a}$$

where A and B are two calibration constants and where

$$\Theta = T(x,z,t) + \Theta(x,z,t=0) \tag{6b}$$

is the absolute temperature (in Kelvin) at this location. If the same surface is opaque but not black, this tension becomes

$$V(x,z,t) = \varepsilon_{\mathrm{sw}}(x,z)V^{\circ}(\Theta) + (1 - \varepsilon_{\mathrm{sw}}(x,z))K_{\mathrm{sw}}E_{\mathrm{sw}}, \tag{6c}$$

where $\varepsilon_{\mathrm{sw}}$ designates the local surface emissivity in the [3.5–5.6 μm] (short wave) spectral detection band of the camera and in the surface – camera direction. E_{sw} is the ambient radiation incident on the scanned surface in the same spectral interval and K_{sw} a calibration constant that takes into account the linear radiative flux/tension response of the camera.

In practical experiments, when starting an experiment from thermal equilibrium, the reflected (steady state) term in Eq. (6c) has not to be known if only the increase of tension is used:

$$\Delta V = V(x,z,t) - V(x,z,0) = \varepsilon_{sw}(x,z)(V^{\circ}(\Theta) - V^{\circ}(\Theta_0)) \quad (6d)$$

with

$$\Theta_0 = \Theta(x,z,0).$$

The $\Delta V(x,z,t)$ signal, averaged over a horizontal width $2L' < 2L$ where transfer can be assumed as 1D in the vertical x direction, will be used to estimate the instantaneous heat transfer coefficient. Either a local (h) or a global ($\bar{h}$) transfer coefficient that includes natural convection and linearized radiation to the surrounding environment, will be looked for:

$$h(x,t) = \varphi(x,t)/T(x,t), \quad (7a)$$

$$\bar{h}(t) = \bar{\varphi}(t)/\bar{T}(t), \quad (7b)$$

where the bar over the h, φ and T quantities designate averages over the vertical dimension x of the foil (x varying from 0 to H). We assume here that the air temperature remains constant and equal to the initial temperature of the slab (this is the zero level for T). Two different estimation techniques will be described next for the calculation of the transfer coefficient starting from the infrared camera measurements.

4.2. First estimation technique: normalized signal

4.2.1. Normalized signal and its model

When the foil emissivity ε_{sw} is not known, it is not possible to invert Eq. (6d) to get an experimental value of temperature T, solution of Eqs. (4a)–(4e) – 1D model – or of Eq. (5) – lumped body model.

First the local ΔV signal that has been averaged over the horizontal direction – see Eq. (6d) – is linearized with respect to temperature Θ

$$\Delta V(x,t) = \varepsilon_{sw}K_1(\Theta(x,t) - \Theta(x,0)) = \varepsilon_{sw}K_1T(x,t). \quad (8a)$$

This is possible if we assume that emissivity ε_{sw} is uniform over the foil surface and if the temperature increase at each location is not too high (lower than 15 °C) in practice), that is for moderate heating of the foil. $K_1(= dV^{\circ}/d\Theta)$ is the derivative of the calibration law (6a), at near ambient temperature.

Integration of Eq. (8a) over the vertical (x) direction, gives rise to an average tension variation

$$\Delta\bar{V}(t) = \varepsilon_{sw}K_1\bar{T}(t). \quad (8b)$$

In purely transient experiments the $q(t)$ excitation reaches a steady level q_∞ after some time, which means that all local or global quantities reach an asymptotic constant level for long times. If a '∞' subscript is used for these asymptotic quantities, the long times average temperature variation (8b) becomes

$$\Delta\bar{V}_\infty = \varepsilon_{sw}K_1\bar{T}_\infty. \quad (8c)$$

This value will be used to normalize the local (8a) or average signal (8b), and consequently to make the emissivity disappear:

$$V^*(x,t) = \Delta V(x,t)/\Delta\bar{V}_\infty = T(x,t)/\bar{T}_\infty = T^*(x,t), \quad (9a)$$

$$\bar{V}^*(t) = \Delta\bar{V}(t)/\Delta\bar{V}_\infty = \bar{T}(t)/\bar{T}_\infty = \bar{T}^*(t), \quad (9b)$$

where T^* or $\bar{T}^*$ is the local or average normalized temperature. The local normalized temperature can be calculated using a Fourier finite cosine transformation – see Eqs. (4a)–(4e):

$$T^*(x,t) = \frac{1}{H}\left(\theta_0^*(t) + 2\sum_{n=1}^{\infty}\theta_n^*(t)\cos(\alpha_n x)\right) \quad (10a)$$

with

$$\theta_0^*(t) = \frac{\theta_0(t)}{\bar{T}_\infty} = \frac{H}{\tau_\infty}\int_0^t (q^*(u) - \phi_0^*(u))\,du \quad (10b)$$

and

$$\theta_n^*(t) = \frac{\theta_n(t)}{\bar{T}_\infty} = -\frac{H}{\tau_\infty}\int_0^t \phi_n^*(u)\exp(-\alpha_n^2(t-u))\,du, \quad (10c)$$

where

$$q^*(t) = q(t)/q_\infty, \quad \phi_n^*(t) = \frac{\phi_n(t)}{\phi_0(\infty)} = \frac{\phi_n(t)}{Hq_\infty} \quad (10d)$$

and where $\tau_\infty(= \rho ce/\bar{h}_\infty)$ is the characteristic time of the foil, related to the steady state asymptotic global heat transfer coefficient $\bar{h}_\infty$.

The derivation of Eqs. (10b) and (10d) has used the following properties of the steady state regime

$$q_\infty = \bar{\varphi}_\infty = \bar{h}_\infty\bar{T}_\infty = \phi_0(\infty)/H. \quad (10e)$$

In a very similar way the average normalized temperature derives directly from the lumped body model – Eq. (5)

$$\bar{T}^*(t) = \frac{1}{\tau_\infty}\int_0^t (q^*(u) - \bar{\varphi}^*(u))\,du, \quad (11a)$$

where

$$\bar{\varphi}^*(t) = \bar{\varphi}(t)/\varphi_\infty = \phi_0^*(t). \quad (11b)$$

One can notice that the lumped body model (11a) corresponds, within the H factor, to the zero harmonic of the 1D model (10b).

4.2.2. Estimation of the time constant

We assume here that, for long enough times after the start of heating of the foil with a constant power, the instantaneous global heat transfer coefficient defined by Eq. (7b) reaches its asymptotic value $\bar{h}_\infty$, while the average wall flux density and temperature are still varying. This assumption is valid in the case of small temperature differences between a wall and a surrounding fluid en-

vironment: a constant steady state heat transfer coefficient can be used for such 'soft' transient problems (quasi steady state approximation). The preceding time constant τ_∞ corresponds to this asymptotic steady state coefficient $\bar{h}_\infty$.

As soon as this regime takes place (constant transfer coefficient after a time $t_{\min}$), the lumped body heat equation becomes

$$\frac{\mathrm{d}\bar{T}}{\mathrm{d}t}+\frac{\bar{h}_\infty}{\rho ce}\bar{T}=\frac{q(t)}{\rho ce}. \tag{12a}$$

Its normalized solution is

$$\bar{T}^*(t)=\bar{T}^*(t_{\min})\exp(-t/\tau_\infty)+\frac{1}{\tau_\infty}\int_{t_{\min}}^{t} q^*(u)\times\exp(-(t-u)/\tau_\infty)\,\mathrm{d}u. \tag{12b}$$

In the case where $q^*(t)=1$ (real Heaviside excitation), this solution becomes

$$\bar{T}^*(t)=\bar{T}^*(t_{\min})\exp(-t/\tau_\infty)+1-\exp(-(t-t_{\min})/\tau_\infty). \tag{12c}$$

If $t_{\max}$ is the time when measurements stop, it is possible to find an estimate $\hat{\tau}_\infty$ $(t_{\min})$ of the time constant τ_∞ for a given value of $t_{\min}$ through a least square model applied to the measurements and to model (12c) on the $[t_{\min}\,t_{\max}]$ interval. The least square sum can be plotted versus $t_{\min}$. The optimum estimate $\hat{\tau}_\infty$ corresponds to the minimum of this residuals curve. The steady state global heat transfer coefficient can be estimated then: $\hat{\bar{h}}_\infty=\hat{\tau}_\infty/\rho ce$.

4.2.3. Estimation of the heat transfer coefficient

Estimation of the heat transfer coefficient requires the estimation of the normalized heat flux starting from the normalized signal (10a) or (11a). This can be done for the average model where Eq. (11a) can be discretized:

$$\bar{T}^*=\begin{bmatrix}\bar{T}^*(t_1)\\ \bar{T}^*(t_2)\\ \vdots\\ \bar{T}^*(t_{i_{\max}})\end{bmatrix}=\frac{\Delta t}{\tau_\infty}\begin{bmatrix}1 & 0 & \cdots & 0\\ 1 & 1 & 0\cdots & 0\\ 1 & 1 & \ddots & \vdots\\ 1 & 1 & \cdots & 1\end{bmatrix}\begin{bmatrix}\beta_1\\ \beta_2\\ \vdots\\ \beta_{i_{\max}}\end{bmatrix}=\mathbf{X}_0\beta \tag{13a}$$

with

$$\beta_i=q^*(t_i)-\bar{\varphi}^*(t_i),\quad 1\leqslant i\leqslant i_{\max}\text{ and }t_i=i\Delta t, \tag{13b}$$

where Δt is the acquisition time step. Since this problem is linear an ordinary least square estimation can be used

$$\hat{\beta}=(\boldsymbol{X}_0^t\boldsymbol{X}_0)^{-1}\boldsymbol{X}_0\bar{\boldsymbol{V}}^*=\boldsymbol{X}_0^{-1}\bar{\boldsymbol{V}}^*, \tag{13c}$$

where $\bar{\boldsymbol{V}}^*$ is the vector of the normalized average tension differences produced by the camera – see Eq. (9b). The measurement, at the same times, of the electrical power allows the calculation of $q^*(t)$ and produces therefore an estimation of the average normalized wall heat flux components $\bar{\varphi}^*(t_i)$ at times t_i. The global heat transfer coefficient can be estimated at the same time

$$\hat{\bar{\boldsymbol{h}}}(t_i)=\hat{\bar{\boldsymbol{h}}}_\infty\hat{\bar{\boldsymbol{\varphi}}}^*(t_i)/\langle\bar{V}^*\rangle_i\quad\text{with}$$
$$\langle\bar{V}^*\rangle_i=\frac{1}{2}(\bar{V}^*_{i-1}+\bar{V}^*_i). \tag{13d}$$

The local heat transfer coefficient can be estimated thanks to the estimation of the local normalized heat flux. This can be calculated starting from an estimation of its harmonics ϕ_n^* – see Eqs. (10b) and (10c). For the zeroth harmonics, one has

$$\hat{\boldsymbol{\phi}}_0^*(t_i)=\hat{\bar{\boldsymbol{\varphi}}}^*(t_i). \tag{14a}$$

The harmonics $\phi_n^*(t)$ are estimated thanks to Eq. (10c) that can be discretized the same way as Eq. (13a)

$$\boldsymbol{\theta}_n^*=\boldsymbol{X}_n\boldsymbol{\phi}_n^*. \tag{14b}$$

A least square method is used for inverting Eq. (14b)

$$\hat{\boldsymbol{\phi}}_n^*=(\boldsymbol{X}_n^t\boldsymbol{X})_n^{-1}\boldsymbol{X}_n^t\boldsymbol{\theta}^*_{n\exp}=\boldsymbol{X}_n^{-1}\boldsymbol{\theta}^*_{n\exp}, \tag{14c}$$

where the experimental values $\theta^*_{n\exp}(t_i)$ of the harmonic of the normalized temperature at time t_i is evaluated through a numerical quadrature (in space) of the normalized local signal – see Eq. (4b)

$$\theta^*_{n\exp}(t_i)=\sum_{k=1}^{k_{\max}}\langle V^*\rangle_{ki}\cos(\alpha_n x_k)\Delta x\quad\text{with}$$
$$\langle V^*\rangle_{ki}=\frac{1}{2}(V^*(x_k,t_{i-1})+V^*(x_k,t_i)), \tag{14d}$$

where Δx is the vertical space step and x_k the vertical position of the kth line of the thermographic frame.

Reconstruction of the local normalized flux density $\varphi^*(x,t)$ is implemented through Fourier cosine inversion of the normalized harmonics $\hat{\boldsymbol{\phi}}_n^*(t)$ and the local heat transfer coefficient $h(x,t)$ is estimated using the same form as Eq. (13d), but on a local basis.

4.3. Second estimation technique: absolute signal

If the foil emissivity ε_{sw} is known, no linearization nor normalization is required any more since inversion of Eq. (6d) provides the local temperature Θ. The average temperature $\bar{T}(t)$ or of the local temperature $T(x,t)$ can therefore be measured. Estimation of $\bar{\varphi}(t)$ and of $\varphi(x,t)$ are implemented the same way as in Section 4.2, which allows an estimation of the global and local coefficients:

$$\hat{\bar{h}}(t_i) = \frac{2\hat{\bar{\varphi}}(t_i)}{\bar{T}(t_i) + \bar{T}(t_{i-1})} \tag{15a}$$

$$\hat{h}(x_k, t_i) = \frac{2\hat{\varphi}(x_k, t_i)}{T(x_k, t_i) + T(x_k, t_{i-1})}. \tag{15b}$$

This technique does not limit the level of heating since no linearization is used anymore. If the emissivity ε_{lw} of the foil in the 10 μm wavelength band (long wave of the ambient emission) is known, it is possible to estimate the convective component h_{conv} of the heat transfer coefficient, using a linearization of its radiative contribution with respect to the difference of temperature between the foil and the surrounding environment

$$\hat{\bar{h}}_{conv}(t) = \hat{\bar{h}}(t) - 4\varepsilon_{lw}\Theta_m^3\bar{\sigma}\bar{T}(t) \quad \text{with}$$
$$\Theta_m = \frac{1}{2}(\Theta_0 + \bar{\Theta}(t)) \cong \Theta_0. \tag{15c}$$

5. Reference conductive model

If one heats a wall in a transient way, starting from thermal equilibrium, the surrounding air layer acts, for very short times, as a semi-infinite medium where heat is transferred by conduction only. In this phase the mechanical inertia of the air layers in the neighbourhood of the wall prevents any instantaneous start of natural convection, which means that heat conduction is the dominant mode of heat transfer. The following relationship can be established [12] between wall temperature and wall flux density of a semi-infinite medium in 1D transient conduction

$$\tilde{T}(p) = \frac{1}{b_{air}\sqrt{p}}\tilde{\varphi}(p), \tag{16a}$$

where the upper tilda stands for the Laplace transform: $\tilde{T}(p)$ and $\tilde{\varphi}(p)$ are the Laplace transforms of the wall temperature $T(t)$ and of the wall flux density $\varphi(t)$, respectively, p being the Laplace parameter and b_{air} the thermal effusivity of air. Three limiting cases can be considered:

5.1. Uniform step of wall temperature

In that case the temperature of the wall is brought instantaneously to a constant level

$$\left.\begin{array}{ll} T(t) = 0 & \text{for } t < 0 \\ T(t) = T_0 & \text{for } t \geqslant 0 \end{array}\right\} \Rightarrow \tilde{T}(p) = \frac{1}{p}T_0. \tag{16b}$$

Eq. (16a) can be inverted and the heat transfer coefficient can be calculated

$$\varphi(t) = \frac{b_{air}}{\sqrt{\pi t}}T_0 = h(t)T_0 \Rightarrow h(t) = \frac{b_{air}}{\sqrt{\pi t}}. \tag{16c}$$

5.2. Uniform step in heat flux density

In that case the wall heat flux density level is brought instantaneously to a constant level

$$\left.\begin{array}{ll} \varphi(t) = \varphi_0 & \text{for } t \geqslant 0 \\ \varphi(t) = 0 & \text{for } t < 0 \end{array}\right\} \Rightarrow \tilde{\varphi}(p) = \frac{1}{p}\varphi_0. \tag{16d}$$

Eq. (16a) can be inverted and the heat transfer coefficient can be calculated

$$T(t) = \frac{2\sqrt{t}}{\sqrt{\pi}b_{air}}\varphi_0 = \frac{1}{h(t)}\varphi_0 \Rightarrow h(t) = \frac{b_{air}\sqrt{\pi}}{2\sqrt{t}}. \tag{16e}$$

5.3. Capacitive coupling with the solid wall

In the type of experiment we are interested in, the wall heat flux $\varphi(t)$ differs from the excitation by Joule effect $q(t)$. This is common to all physical transfer situations where there is a coupling between solid wall and air layer heat transfers – see [7] for example. The simple lumped body heat balance, already written in Eq. (4a) for $n = 0$, can be transformed into the Laplace domain, which yields

$$\rho ce\, p\tilde{T}(p) = \tilde{q}(p) - \tilde{\varphi}(p). \tag{16f}$$

The coupling between the two media – Eqs. (16a) and (16f) – can be represented by the capacity/impedance network [12] shown in Fig. 3. It allows the calculation of Laplace transforms of wall temperature and flux. These transforms can be analytically inverted [13], which yields the time variation of the heat transfer coefficient:

$$h(t) = \rho ce K^2 \frac{1 - \exp(K^2 t)\ \mathrm{erfc}(K\sqrt{t})}{\frac{2K\sqrt{t}}{\sqrt{\pi}} - (1 - \exp(K^2 t)\ \mathrm{erfc}(K\sqrt{t}))} \tag{16g}$$

with

$$K = \frac{b_{air}}{\rho ce}.$$

This shows that in this situation the transient "conductive" heat transfer coefficient is not an intrinsic property

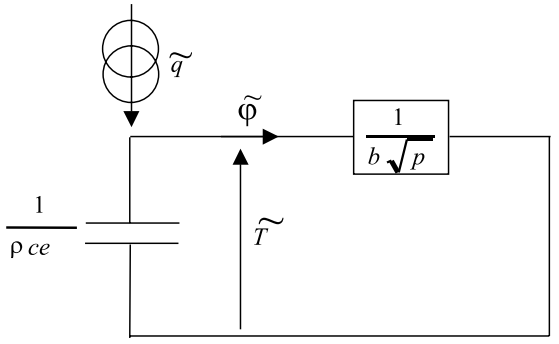

Fig. 3. Coupled capacitive model – impedance network.

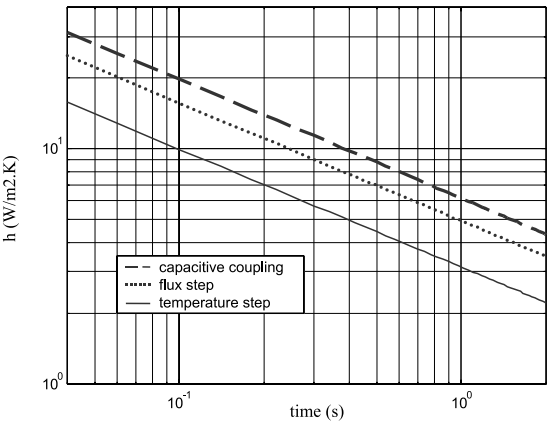

Fig. 4. Three conductive models for the global heat transfer coefficient ($b_{air} = 5.6$ J m^{-2} K^{-1} s$^{-1/2}$ – $K = 0.1573$ s$^{-1/2}$).

of the fluid since it depends on the capacity (per unit area) of the wall ρce. The transfer coefficient variation with time, of the three conductive models (16c) – constant temperature (a) – (16e) – constant flux (b) – and (16g) – coupled model (c) – are plotted in Fig. 4 (log–log scales). It is interesting to notice that the coupled model does not lie in between the two preceding "classical" models as a too rapid first guess should have been.

6. Simulation results

In order to be confident in the results of an experimental estimation, it is very important to test the inversion algorithm on simulated data [14].

The test function, for the variation of the local heat transfer coefficient, was chosen as

$$h(x,t) = \left(\bar{h}_\infty + \frac{b_{air}\sqrt{\pi}}{2\sqrt{t}}\right)\frac{3}{4}\left(\frac{x}{H}\right)^{-1/4} = h_t(t)h_x(x). \quad (17a)$$

The first factor, $h_t(t)$, corresponds to the sum of a constant flux conductive transfer in air, see Eq. (16e), valid for short times, and of the usual steady state global heat transfer coefficient, valid for long times ($\bar{h}_\infty = 6$ W m^{-2}K^{-1}; $b_{air} = 5.6$ S.I.). The second factor, $h_x(x)$, corresponds to the laminar natural convection heat transfer coefficient x-distribution along a vertical flat plate (local Nusselt number varying as the Grashof number at the 1/4 power). It has been normalized to get a unit integral on the plate height H. In order to solve the direct problem, the truncated spectrum $\phi = [\phi_0\phi_1 \cdots\cdots \phi_N]^t$ of the heat losses – see Eq. (4b) has to be expressed in terms of the temperature spectrum $\boldsymbol{\theta} = [\theta_0\theta_1 \cdots\cdots \theta_N]^t$ and of the spectrum of the heat transfer coefficient (17a). The harmonics of h_x can be calculated by a numerical summation of the following integral, discretized over the pixel height Δx

$$h_n = \int_0^h h_x(x)\cos(\alpha_n x)\,dx \cong H^{1/4}\sum_{k=1}^{k_{max}}\left[\left(x_k + \frac{\Delta x}{2}\right)^{3/4} - \left(x_k - \frac{\Delta x}{2}\right)^{3/4}\right] \times \cos(\alpha_n x_k)\Delta x. \quad (17b)$$

The resulting expression is

$$\phi(t) = h_t(t)\boldsymbol{M}\ \boldsymbol{\theta}(t), \quad (17c)$$

where $\boldsymbol{M}$ is a $(N+1)x(N+1)$ square convolution matrix – see [12, Section 6.2] – whose coefficients depend on the harmonics h_n of the space part h_x of h – see Eq. (17d).

Eq. (4a) becomes then

$$\frac{d\boldsymbol{\theta}}{dt} = -\left(A + \frac{h_t(t)}{\rho ce}M\right)\boldsymbol{\theta} + S(t), \quad (17d)$$

where A is a diagonal matrix and S a vector with

$$A_{nq} = a\alpha_n\delta_{nq}, \quad S_n(t) = \delta_{0n}\frac{H}{\rho ce}q(t). \quad (17e)$$

System (17d) is solved by a Runge–Kutta method and the $T(x, t)$ field is reconstructed using Eq. (4c). An additive gaussian noise, of $\sigma = 0.1$ °C standard deviation, is added to the temperature. The corresponding temperature distributions, for three different locations and for the average temperature, are plotted in Fig. 5(a) (for a step excitation $q(t) = 120$ W m^{-2}). Inversion of these simulated data is implemented according to the first estimation method described in Section 4.2.

The estimated global transfer coefficient variation with time is plotted in Fig. 5(b). It is very close to the exact curve, even if a slight bias can be noticed for long times (not visible in this curve, but appearing for longer times): it is caused by the normalization that cannot be done with asymptotic values but with values at the end of the recording (one has used here $\bar{T}^*(t) = \bar{T}_{exp}(t)/\bar{T}_{exp}(t = 55\text{ s})$, $\bar{T}_{exp}$ being the experimental simulated data). This result in a estimated time constant $\hat{\tau}_\infty (= 5.40$ s) slightly lower than its exact value $\tau_\infty (= 5.47$ s). One can notice that no regularization method has been needed to get the estimated values $\hat{\bar{\boldsymbol{\varphi}}}(t)$ and $\hat{\bar{\boldsymbol{h}}}(t)$ of the two functions: this is due to the fact that, in the y direction, the inverse problem is well posed since $\varphi(t)$ is estimated at the same location as the place where the data (temperatures) are measured.

Since the $h_x(x)$ space distribution, even filtered by the local averaging of the Fourier series expansion – see Eq. (17b) – has a spectrum characterized by a high content in high frequency components, calculation of the harmonics of high order of the experimental signal – Eq. (14d) – cannot be done with a good enough precision (with this signal over noise ratio of 200) to reconstruct the heat loss flux if noise is present in the simulated data. This effect is shown in Fig. 5(c).

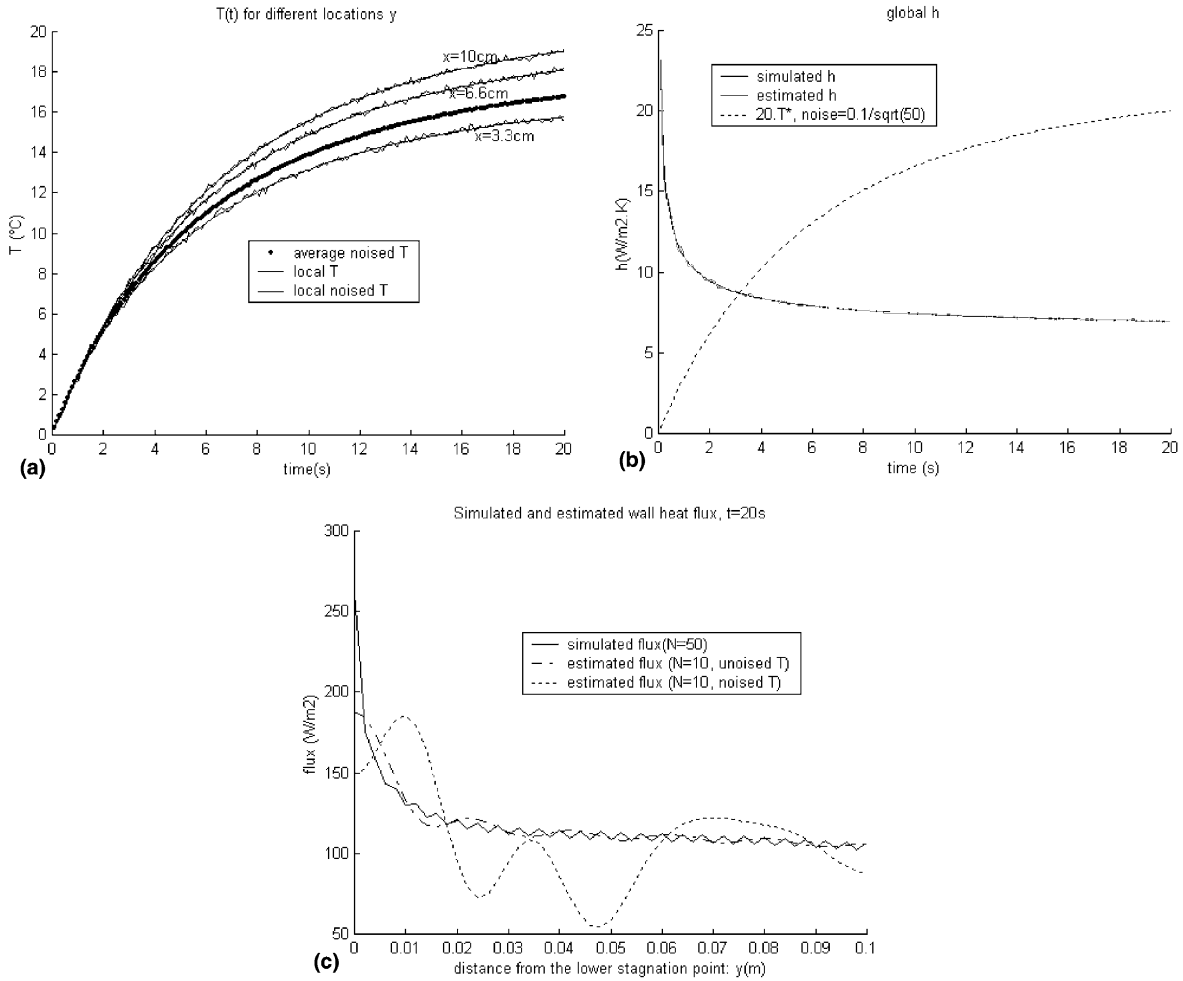

Fig. 5. (a) Simulated temperatures starting from a given h function – $h(x,t) = h_t(t)h_x(x)$ – and a given step heat stimulation with $q = 120$ W m^{-2}, noised by an additive random noise of standard deviation $\sigma = 0.1$ °C. (b) Estimated global heat transfer coefficient $\bar{h}(t)$, starting from simulated experiments. (c) Estimated local wall heat flux density $\varphi(x,t)$, at time $t = 20$ s, starting from simulated experiments.

Only a space regularization would allow to reconstruct the shape of the h distribution in the lower part of the wall, because of the infinite level of this coefficient and of its derivative at the stagnation point $y = 0$. In order to get a realistic reconstruction of this distribution, the regularization technique would require a a priori information on its shape, which is not what is looked for here.

7. Experimental results

Four experiments, numbered 1–4 have been made with a heating power q of 120 W m^{-2}. They correspond to two different acquisition periods Δt of the camera and to two different states for the surface of the foil – see Table 1.

Table 1
Heating experiments with a 120 W m^{-2} Joule dissipation

Experiment	Δt (ms)	Surface state	$\hat{\tau}_\infty$ (s)	$\hat{\bar{h}}_\infty$ (W m^{-2} K^{-1})
1	160	Uncleaned	5.2	6.7
2	40	Uncleaned	5.0	7.0
3	160	Cleaned	5.2	6.8
4	40	Cleaned	5.2	6.8

It has been noticed that, without a cleaning of the foil's surface, the thermal signal did not appear uniform on a horizontal line. This can be caused by the presence of surface contaminants (grease...) that yield a non-uniform emissivity. So experiments with an acetone cleaned surface have also been made.

7.1. First estimation technique

The first estimation technique (normalized signal) has been implemented. The normalized experimental thermograms are shown in Fig. 6 and the corresponding estimated time constants and asymptotic $\bar{h}_\infty$ values are given in Table 1. The short acquisition period experiments (numbered 2 and 4) yield the lowest residuals (of the order of 2/1000 of the asymptotic $T^* = 1$ normalized signal). A recording of the measured power (for $q_\infty = 1228\ \mathrm{W\ m^{-2}}$) is shown in Fig. 7(a). Because of the temperature dependent electrical resistivity of the graphite foil, one can notice a 3% power decrease between the start of the heating and the quasi-steady state regime. Even if the stimulation does not constitute a rigourous step heating, this effect is taken into account by the model (12b). The normalized power $q^*(t)$ is shown in Fig. 7(b) for the four experiments while the estimated reduced wall flux density $\bar{\varphi}^*(t)$ and the corresponding global heat exchange coefficient $\bar{h}(t)$ are given in Figs. 8(a) and (b). It is important to notice that the steady state wall heat flux is reached only 15 s after heating has started and that the h coefficient requires about 3 or 4 s to get a constant value.

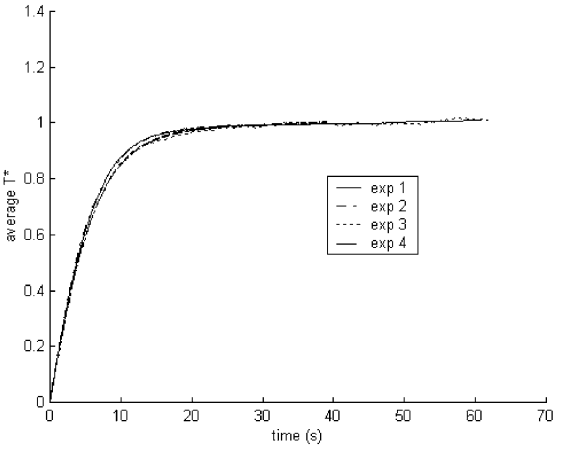

Fig. 6. Experimental normalized thermograms $\bar{T}^*(t) = \bar{V}^*(t)$, for experiments 1–4.

7.2. Second estimation technique

The normalized signal technique is characterized by an experimental bias: as time goes on, the two lateral copper bars behave as heat sinks that contribute to evacuate heat from the central portion of the foil. It therefore adds a second time constant, linked to their inertia, to the experimental signal, and the long time constant asymptotic temperature level is not reached, even after a time equal to 10 τ_∞. This long times bias affects also the short time estimated h values because of the normalization. Another bias linked to this technique is caused by the linearity assumption (signal versus temperature). The temperature rise related to experiments 1–4 is of the order of 15 °C which is a upper limit for this assumption. In order to get rid of these limitations the hemispheric spectral emissivity of the foil has been measured and its value in the two interesting spectral bands are given in Table 2.

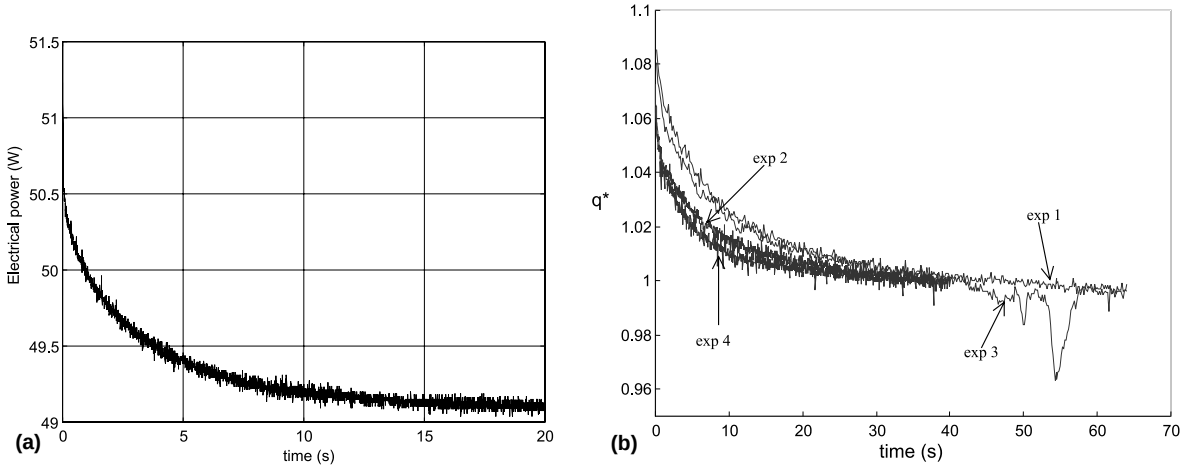

Fig. 7. (a) Variation with time of the power $w(t)$ dissipated in the foil. (b) Variation with time of the normalized power $\bar{q}^*(t)$, for experiments 1–4.

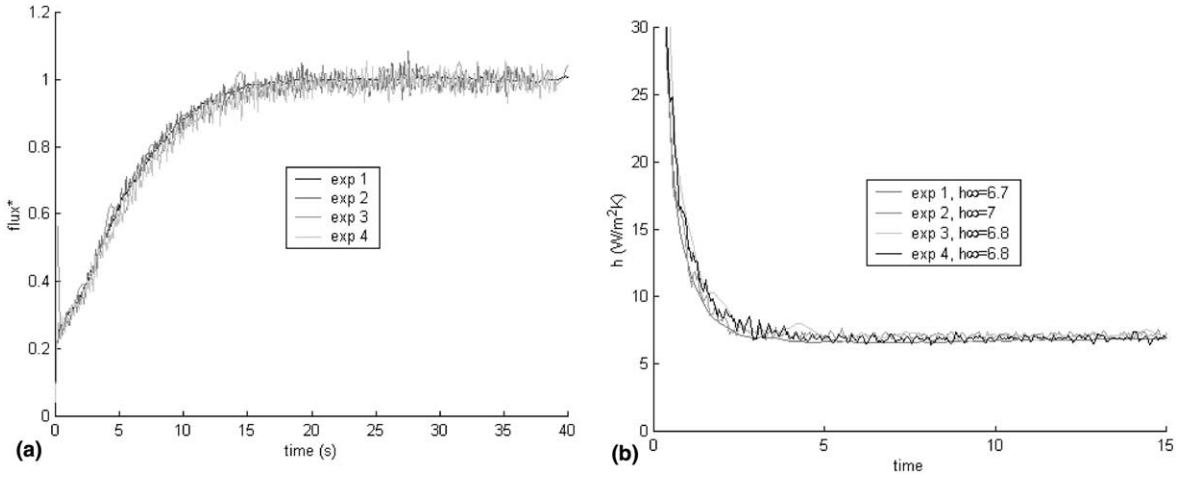

Fig. 8. (a) Estimated normalized average wall heat flux density $\bar{\varphi}^*(t)$, for experiments 1–4. (b) Estimated global heat transfer coefficient $\bar{h}(t)$, for experiments 1–4.

Table 2
Hemispheric emissivity of the graphite foil

Foil	ε_{sw} [3.5–5.6 μm]	ε_{lw} [10 μm]
Uncleaned	0.60	0.57
Cleaned	0.59	0.55

The estimated $h(t)$ variations, calculated by the two techniques are compared in Fig. 9 for experiment 2. The second technique (absolute signal) yields higher $\bar{h}$ values that are not affected by the copper bar bias at short times.

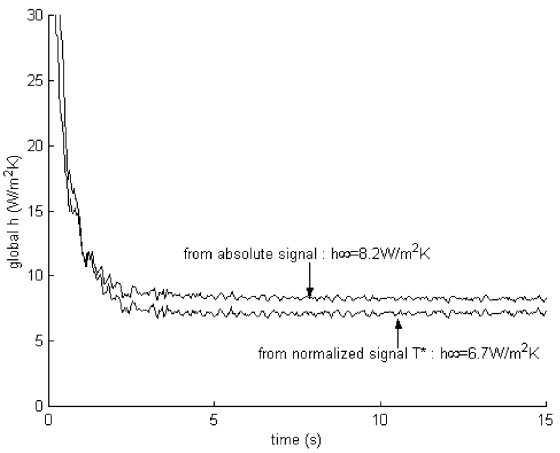

Fig. 9. Comparison of the global heat transfer coefficient estimated by the two different estimation techniques, for experiment 2.

7.3. Effect of the level of the stimulation

Because of the sharp decrease of the estimated coefficient for the early times, it is interesting to plot its variation in a log–log scale. The estimated $\bar{h}$ values – representing natural convection alone, see Eq. (15c) – for experiment 2, are plotted in Fig. 10 (second estimation technique). They correspond to a heating level $q_\infty = 120$ W m^{-2} that is related to a Rayleigh number (based on the foil's height H) $Ra = 4.3 \times 10^7$. Two asymptotic stages can be distinguished: a quasi linear decrease for short times and a constant level for long times. The slope of the linear part is equal to −0.89. This value has a low precision, since it is obtained by a least square

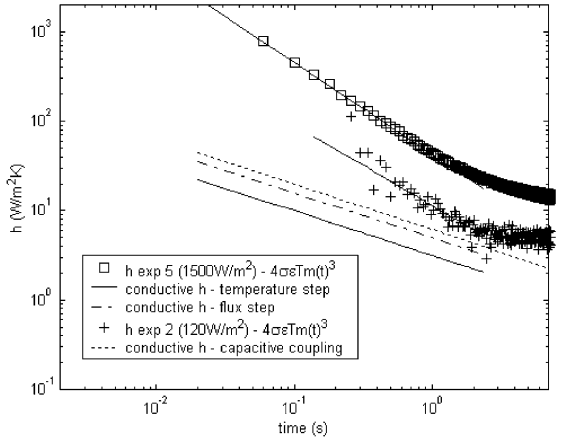

Fig. 10. Estimation of the global convective transfer coefficient $\bar{h}_{conv}(t)$ – for two levels of step heating $q = 120$ W m^{-2} (experiment 2) and $q = 1500$ W m^{-2} (experiment 5) – and the three reference conductive models.

technique and is associated to the high dispersion of the first estimates obtained at short times. In order to get a better signal over noise ratio, experiment 5 ($\Delta t = 40$ ms, cleaned foil) has been implemented with a higher value of the solicitation ($q_\infty = 1500$ W m^{-2} – $Ra = 5.4 \times 10^8$). The corresponding points are plotted in Fig. 10. The estimated $\bar{h}$ values are characterized by a lower dispersion and a short times slope of −1.03 can be estimated. It is important to underline that the two estimated slopes for experiments 2 and 5 depart very much from the −0.5 slope associated with the three conductive models also shown in the same figure. The orders of magnitudes are also clearly different: the conductive regime cannot be observed in the scale of time that has been considered by our transient experiment ($t \geqslant 40$ ms).

This observation means that, for short times, transient natural convection cannot be explained by heat conduction in the semi-infinite static air. This result has not been met for water where Goldstein and Eckert [2] produced clear results of an early uniform h variation respecting Eq. (16e) – step wall heat flux. These authors produced also, in the same article, qualitative experimental results (interferograms) of the same experiment in air: these interferograms clearly show that heat transfer is one-directional during about 1 s after heating has started. They did not produce quantitative results for h during this first phase.

Our results tend to show that another phenomenon, different from simple conduction, takes place during this phase. Zappoli et al. [15] have studied numerically the response of a very compressible, low diffusivity, supercritical fluid under zero gravity. They have shown that acoustic effects could lead to a transformation of thermal energy into kinetic energy in a hot expanding boundary layer (the piston), which in turn is transformed in the bulk into internal energy. This resulted in very important heat transport, completed after about 1% of the diffusion time. In our experiments the diffusion time (based on the thickness of the steady state boundary layer $\delta = 5$ mm) is of the order of 1 s (δ^2/a_{air}). Even if the other conditions are different, one may suspect a mechanism of this type, involving the compressibility of air. Of course this is only a simple assumption that remains to be validated.

7.4. Relaxation experiments

It has been possible to make relaxation experiments with our setup: starting from the steady state regime produced by a constant solicitation q_∞, the electrical heating is turned off and the temperature decrease of the foil is monitored by the infrared camera. The direct model used is

$$\bar{T}(t) = \bar{T}(0) - \frac{1}{\rho c e} \int_0^t \bar{\varphi}(u)\, \mathrm{d}u. \tag{17f}$$

The second technique (absolute signal) is used to estimate the average wall flux density $\bar{\varphi}(t)$ and the $\bar{h}$ coefficient is estimated according to Eq. (15a).

Two experiments have been realized with the cleaned foil and a $\Delta t = 40$ ms acquisition period: experiment 6, starting from a high initial temperature $\bar{T}(0)$ and experiment 7, starting from a low initial temperature.

The variation with time of the measured temperature, of the estimated wall heat flux and of the global transfer coefficient (convection and radiation) are shown in Figs. 11(a) and (b). It can be noticed that the heat transfer

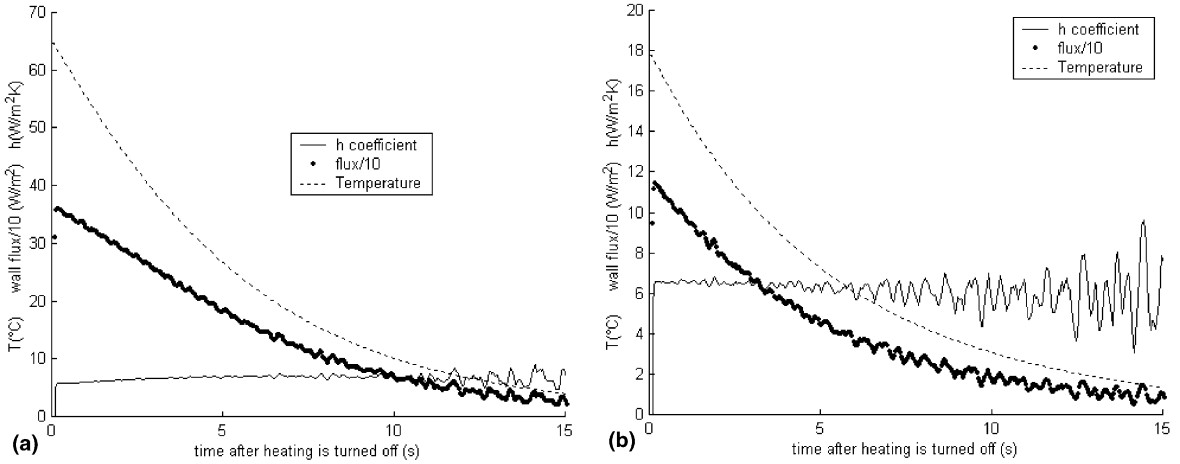

Fig. 11. Relaxation experiments, starting from steady state – temperatures $\bar{T}(t)$, estimated wall heat flux densities $\bar{\varphi}(t)$ and estimated global heat transfer coefficient (convection and radiation) $\bar{h}(t)$: (a) experiment 6 – high initial temperature; (b) experiment 7 – low initial temperature.

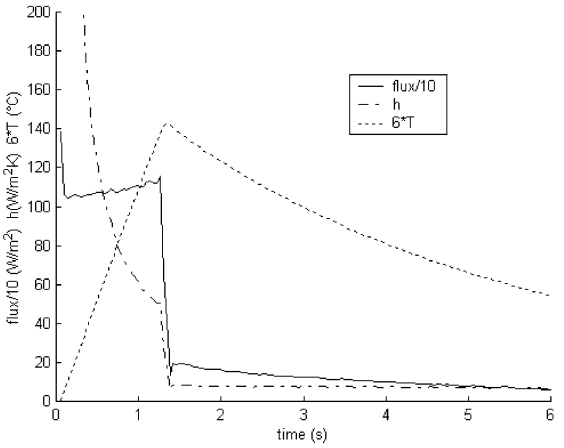

Fig. 12. Temperatures $\bar{T}(t)$, estimated wall heat flux densities $\bar{\varphi}(t)$ and estimated global heat transfer coefficient (convection and radiation) $\bar{h}(t)$ – for a relaxation regime caused by a stop in the transient heating phase – experiment 8.

remains nearly constant in this type of experiment. If the estimated wall heat flux curves of Figs. 8(a) and 11(b) are compared, one notices that the characteristic time to get 50% of the maximum flux is 3.5 s (step heating experiment 2 – Fig. 8) while the corresponding time to get a 50% decrease of the initial flux is 3.9 s (relaxation experiment 7 – Fig. 11(b)): the high initial heat transfer coefficient (step heating) is responsible for this slight difference. This difference is slight because the initial heat transfer coefficient is associated with low temperature differences and therefore to low heat fluxes.

The complete heating and relaxation phase is shown in Fig. 12 – experiment 8 – where heating is stopped after about 1.3 s (time corresponding still to the transient phase of the heat transfer coefficient). One can notice the instantaneous sharp decrease of the heat exchange coefficient: it shows that such a perturbation in the heating procedure does not enhance the heat exchange coefficient.

This seems to show that only local perturbations of the heating mode could maybe increase this coefficient since global time perturbations (on the whole surface) cannot bring much enhancement.

8. Conclusion

Transient heat convection in air, produced by step Joule heating of a very thin vertical graphite foil, has been studied experimentally. Two different methods of inversion have been proposed to estimate the local or global transient heat transfer coefficient, starting from infrared camera measurements. The first method did not require the knowledge of the foil's emissivity but could produce biased results because of the heat losses to the holding bars of the setup. The second method required emissivity measurements but could provide the convective contribution to the measured transfer coefficient. It was demonstrated, by simulation, that the level of the signal over noise ratio of our experiments allows a precise estimation of the global heat exchange, which is not the case for the local coefficient. The theoretical variations with time of the transfer coefficient in the first phase of heating, where conduction is supposed to be the principal mode of exchange, were recalled.

Experimental results, with different levels of heating, show that the early transfer coefficients decrease proportionally to t^{-1}, and not to $t^{-1/2}$ as the early conduction theory would anticipate. Other effects than those already presented in the literature remain to be investigated in order to explain the discrepancy of this theory for air.

Relaxation experiments, starting either from a steady or a transient situation, have shown that a transient mastering in the heating of the wall as a whole (uniform Joule heating) cannot increase the wall/air exchange. Only local perturbations might enhance such a heat exchange.

Acknowledgements

This work was done within the french AMETH network (Improvement of the Thermal Exchanges).

References

[1] R. Siegel, Transient free convection from a vertical flat plate, Trans. Am. Soc. Mech. Engrs. 80 (1958) 347–359.
[2] R.J. Goldstein, E.R.G. Eckert, The steady and transient free convection boundary layer on a uniformly heated vertical plate, Int. J. Heat Mass Transfer 1 (1960) 208–218.
[3] E.R. Menold, Y. Kwang-Tzu, Asymptotic solutions for unsteady laminar free convection on a vertical plate, ASME J. Appl. Mech. E 84 (1962) 124–126.
[4] J.A. Schetz, R. Eichhorn, Unsteady natural convection in the vicinity of a doubly infinite vertical plate, J. Heat Transfer (November) (1962) 334–338.
[5] R.J. Goldstein, D.G. Briggs, Transient free convection about vertical plates and cylindrical cylinders, J. Heat Transfer (November) (1964) 490–500.
[6] B. Gebhart, Transient natural convection from vertical elements, J. Heat Transfer (February) (1961) 61–70.
[7] B. Gebhart, Transient natural convection from vertical elements – appreciable thermal capacity, J. Heat Transfer (February) (1963) 10–14.
[8] B. Gebhart, D.E. Adams, Measurements of transient natural convection on flat surfaces, J. Heat Transfer (February) (1963) 25–28.
[9] B. Gebhart, Natural convection cooling transients, Int. J. Heat Mass Transfer 7 (1964) 479–483.

[10] B. Sammakia, B. Gebhart, Z.H. Qureshi, Measurements and calculations of transient natural convection in water, J. Heat Transfer 104 (1982) 644–648.
[11] Y. Joshi, B. Gebhart, Transient response of a steady vertical flow subject to a change in surface heating rate, Int. J. Heat Mass Transfer 31 (4) (1988) 743–757.
[12] D. Maillet, S. André, J.-C. Batsale, A. Degiovanni, C. Moyne, Thermal Quadrupoles: Solving the Heat Equation Through Integral Transforms, Wiley, Chichester, 2000.
[13] M. Abramowitz, I.A. Stegun, Handbook of Mathematical Functions, ninth ed., Dover, New York, 1970.
[14] J.V. Beck, B. Blackwell, C.R. St-Clair Jr., Inverse Heat Conduction – Ill-posed Problems, Wiley, Chichester, 1985.
[15] B. Zappoli, D. Bailly, Y. Garrabos, B. Le Neindre, P. Guenoun, D. Beysens, Anomalous heat transport by the piston effect in supercritical fluids under zero gravity, Phys. Rev. A 41 (4) (1990) 2264–2267.